

**NASA  
Technical  
Paper  
2979**

March 1990

# Radiation Exposure for Manned Mars Surface Missions

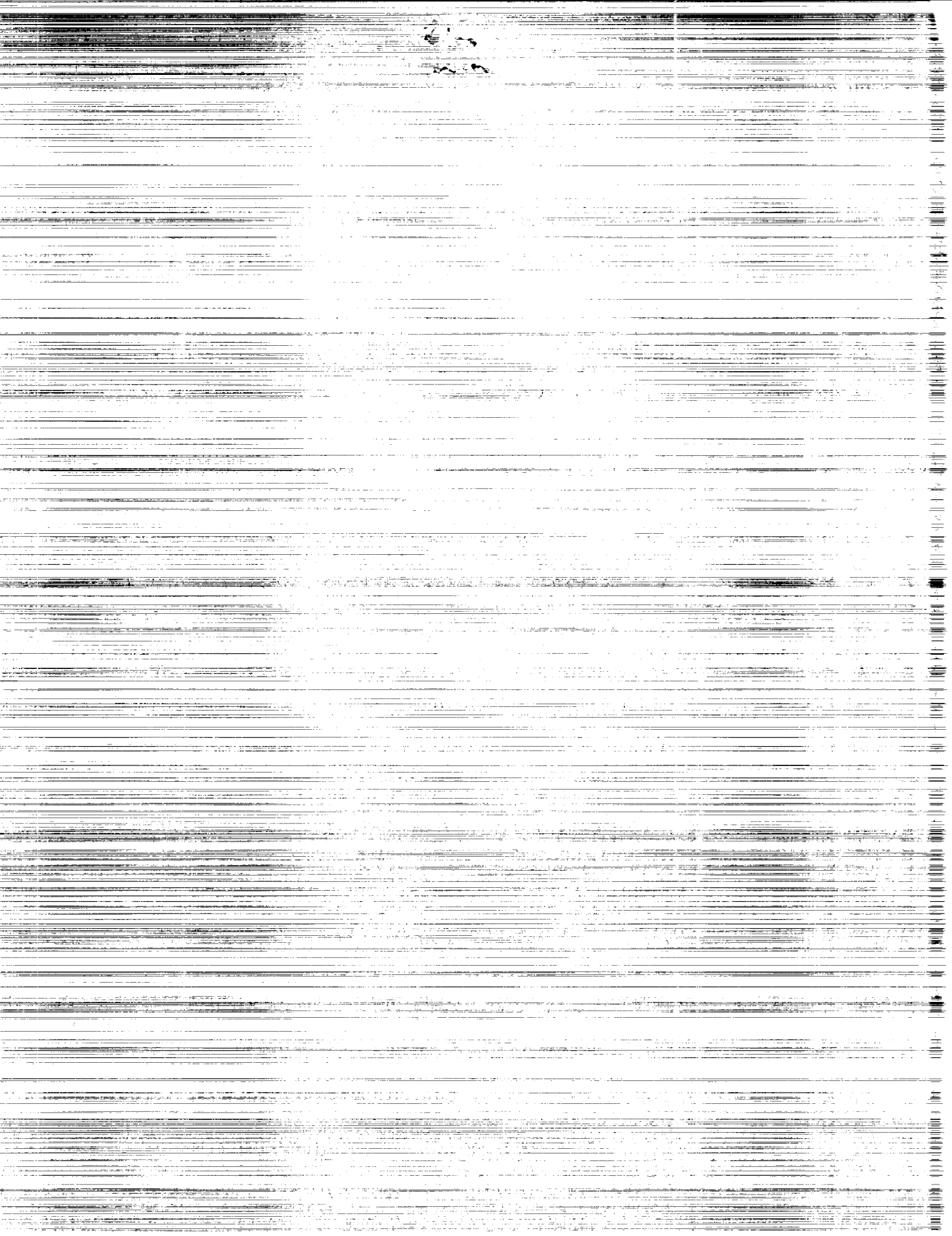
Lisa C. Simonsen,  
John E. Nealy,  
Lawrence W. Townsend,  
and John W. Wilson

(NASA-TP-2979) RADIATION EXPOSURE FOR  
MANNED MARS SURFACE MISSIONS (NASA) 25 p  
CSCL 038

N90-18357

Unclas  
H1/93 0252780

**NASA**



**NASA  
Technical  
Paper  
2979**

1990

# Radiation Exposure for Manned Mars Surface Missions

Lisa C. Simonsen,  
John E. Nealy,  
Lawrence W. Townsend,  
and John W. Wilson  
*Langley Research Center  
Hampton, Virginia*

**NASA**

National Aeronautics and  
Space Administration  
Office of Management  
Scientific and Technical  
Information Division



## Summary

The Langley cosmic ray transport code and the Langley nucleon transport code (BRYNTRN) are used to quantify the transport and attenuation of galactic cosmic rays (GCR) and solar proton flares through the Martian atmosphere. Surface doses are estimated using both a low-density and a high-density carbon dioxide model of the atmosphere which, in the vertical direction, provide a total of 16 g/cm<sup>2</sup> CO<sub>2</sub> and 22 g/cm<sup>2</sup> CO<sub>2</sub> of protection, respectively. Doses are also estimated at altitudes up to 12 km above the Martian surface, where the atmosphere will provide less total protection. At the Mars surface during the solar minimum cycle, a blood-forming organ (BFO) dose equivalent of 10.5 to 12 rem/yr due to galactic cosmic ray transport and attenuation is calculated. These GCR doses do not vary significantly at altitudes up to 12 km because of their penetrating high-energy fluxes. Estimates of the BFO dose equivalents that would have been incurred from the three large solar flare events of August 1972, November 1960, and February 1956 are also calculated at the surface and at altitudes up to 12 km above the Martian surface. Results indicate surface BFO dose equivalents of approximately 2-5, 5-7, and 8-10 rem per event, respectively. Unlike the GCR doses, the solar flare doses are found to vary significantly in the altitude regime investigated. At relatively high (mountaintop) altitudes in the upper atmosphere, the decreased solar flare radiation attenuation results in doses that are significantly greater. At an altitude of 12 km, the radiation BFO dose equivalents are estimated to be 17-30 rem, 14-19 rem, and 13-15 rem for the August 1972, November 1960, and February 1956 events, respectively.

## Introduction

A future goal of the United States space program is a commitment to the manned exploration and habitation of Mars. Once space travelers leave the protective Earth environment, the hazards of space become an important consideration on such missions. One major concern is the damaging effect of ionizing radiation from high energy galactic fluxes and solar proton flares.

Reference Mars mission descriptions have been manifested by the NASA Office of Exploration in their Study Requirements Document (ref. 1). In current scenario descriptions, the flight time to Mars is estimated to take from 7 months to over a year with stay times on the surface ranging from 20 days to 2 years. The crew will encounter the most harmful radiation environment in transit to Mars. Adequate

protection must be provided for this environment. However, once on the surface, the Martian atmosphere should provide a significant amount of protection from the harmful radiative fluxes. The scope of this paper focuses on quantifying the transport and attenuation of galactic cosmic rays during solar minimum conditions and of solar flare protons through the Mars atmosphere to estimate the probable doses received by surface inhabitants. The characterization of this environment is essential in assessing the radiation protection requirements for extended crew durations on the surface.

## Symbols and Abbreviations

BFO	blood-forming organ
BRYNTRN	baryon transport computer code
$c$	number density, particles/unit volume
COSPAR	Committee on Space Research
$D$	absorbed dose, energy/mass
$E$	energy
GCR	galactic cosmic ray
$H$	dose equivalent (eq. (3))
$h$	altitude above Martian surface
$M$	molecular weight
$N_A$	Avogadro's number
$n$	neutrons
$p$	protons
$Q$	quality factor (eq. (3))
$R$	radius of Mars
$S$	stopping power, energy/distance
$s$	distance along slant path
sol	a Martian day
$x$	distance
$Z$	atomic number
$z$	vertical altitude (fig. 20)
$\alpha$	alpha particles
$\theta$	zenith angle (fig. 20)
$\mu$	total nuclear cross section, distance <sup>-1</sup>
$\sigma$	differential interaction cross section, distance <sup>-1</sup> · energy <sup>-1</sup>
$\tau$	absorber areal density, mass/area

$\Phi$  differential flux, particles/  
(area·time·energy)

## Mars Radiation and Physical Environment

The free-space, charged particle environment surrounding Mars comprises a continuous flux of solar wind particles and galactic cosmic ray (GCR) constituents, augmented on occasion by random solar flare events. Since Mars is devoid of an intrinsic magnetic field strong enough to deflect the charged particles, many of these particles are able to reach the outer atmosphere. Ordinary solar wind particles have energies too low to penetrate the atmosphere; however, GCR and energetic flare particles can penetrate the atmosphere.

The GCR constituents are relatively well known with most of the incurred dose resulting from the stripped nuclei of chemical elements. Less is known about the energy distributions of these ions, but enough measurements have been made to specify a working model of these distributions. The GCR flux-energy distribution selected for this analysis is for the minimum of the solar activity cycle or the time of maximum GCR flux as shown in figure 1 (ref. 2). It is believed that these GCR flux intensities do not vary significantly within the area of the solar system occupied by the terrestrial planets, thus this model is directly applied to Mars (ref. 3).

The largest solar flares occur infrequently with one to four events per solar cycle, and a prediction of what may be expected from any given event is difficult. In this analysis, fluence-energy spectra at 1 AU are used for the three largest flares observed in the last half century, which are the events of August 1972, November 1960, and February 1956. In the vicinity of Mars (approximately 1.5 AU), the fluence (time-integrated flux) from these flares is expected to be less. A reasonable estimate is that the radial dispersion of the flare particle flux is inversely proportional to the square of the distance from the Sun (ref. 4). However, large variabilities in this behavior may be expected primarily because of inhomogeneities in the interplanetary magnetic field, anisotropic flux properties, and the nature of the energy spectrum (ref. 5). For the flare calculations in this analysis, the free-space, fluence-energy spectra at 1 AU are conservatively applied to Mars (fig. 2 redrawn from ref. 6).

The Martian atmosphere provides protection from galactic cosmic rays and solar flares, with the amount of protection depending on the atmospheric composition and structure. The composition of the lower atmosphere by volume is approximately 95.3 percent carbon dioxide, 2.7 percent

nitrogen, and 1.6 percent argon. For simplicity in this analysis, the atmosphere is assumed to be 100 percent carbon dioxide. The Committee on Space Research (COSPAR) has used data on the atmospheric structure gathered during the Viking entries to develop the COSPAR warm, high-density and cool, low-density atmosphere models. These models use the daily mean temperatures and pressures at mid-latitude sites during the summer season (ref. 7). The vertical temperature and pressure profiles for the models are shown in figure 3. The low-density model assumes a surface pressure of 5.9 mbar and provides 16 g/cm<sup>2</sup> of carbon dioxide shielding in the vertical direction. The high-density model assumes a surface pressure of 7.8 mbar and provides 22 g/cm<sup>2</sup> of shielding in the vertical direction. Although these models are based on the Northern Hemisphere during the summer season, they represent the best data on the range of temperature and pressure from 100 km to the surface (ref. 8). These two models should provide a good estimate of the possible variation in radiation intensities at the surface.

The specific dose incurred by crew members will vary seasonally as the surface pressure on Mars varies with the condensation and sublimation of the polar ice caps. Also affecting the specific dose incurred will be the elevation of the site. The seasonal variation in pressure and an effect of elevation are shown for the Viking landing sites in figure 4 (ref. 9). The Viking 1 site is 1.5 km below the mean surface level with the pressure varying between 6.8 and 9.0 mbar, and the Viking 2 site is 2.5 km below the mean surface level with the pressure varying seasonally between 7.5 and 10.0 mbar. Thus, the atmosphere provides the greatest protection at lower elevations during times of maximum surface pressure.

The amount of protection provided by the atmosphere can vary greatly at different elevations. The surface of Mars has a great deal of topographical relief and a great variety of surface features including craters, channels, valleys, fluvial features, and volcanic features. Since Mars has no sea level against which to measure elevation, an artificial datum has been established approximately 1.8 km below the mean surface elevation (ref. 7). The large variation in the average elevation of the surface for the different latitude belts is illustrated in figure 5 (ref. 10). The largest crater, Hellas Planitia, reaches more than 4 km below the datum. Hundreds of kilometers of channels, flat-floored winding valleys, and steep-walled canyons reaching over 7 km deep exist on the surface. Extremely high regions can also be found. Tharsis Bulge covers nearly one-quarter of the planet with a summit at an elevation over 11 km above the datum. The largest volcano, Olympus Mons, has

a summit 27 km above the datum. In the lowest regions, the radiation dose estimates will be conservative. However, at the very high altitudes, the atmosphere will provide considerably less shielding; therefore, dose predictions for altitudes of 4 km, 8 km, and 12 km are included in the analysis.

## Radiation Transport and Dosimetry Analysis

The NASA Langley Research Center nucleon and heavy ion transport computer codes are used to predict the propagation and interactions of the free-space nucleons and heavy ions through the carbon dioxide atmosphere. For large solar flare radiation, the baryon transport code BRYNTRN (ref. 11) is used. For the galactic cosmic rays, an existing heavy ion transport code is integrated with the BRYNTRN code to include the transport of high-energy heavy ions up to atomic number 28 (refs. 12 and 13). Both codes solve the fundamental Boltzmann transport equation in the one-dimensional, or "straight ahead," approximation form:

$$\left[ \frac{\partial}{\partial x} - \frac{\partial}{\partial E} S_j(E) + \mu_j(E) \right] \Phi_j(x, E) = \sum_{k>j} \int_E^{\infty} \sigma_{jk}(E, E') \Phi_k(x, E') dE' \quad (1)$$

where the quantity to be evaluated,  $\Phi_j(x, E)$ , is the flux of particles of type  $j$  having energy  $E$  at spatial location  $x$ . The solution methodology of this integrodifferential equation may be described as a combined analytical-numerical technique (ref. 14). The accuracy of this numerical method has been determined to be within approximately 1 percent of exact benchmark solutions (ref. 15). The data required for solution consist of the stopping power  $S_j$  in various media, the macroscopic total nuclear cross sections  $\mu_j$ , and the differential nuclear interaction cross sections  $\sigma_{jk}$ . The differential cross sections describe the production of type  $j$  particles with energy  $E$  by type  $k$  particles of energies  $E' > E$ . Detailed information on these data base compilations is described in references 11, 16, and 17.

The present GCR code formulation is considered to be an interim version, since some features of the transport interaction phenomena have yet to be incorporated. These include improvements and additions to the existing nucleus-nucleus cross sections and their energy dependence, and provisions for pion and muon contributions. Further improvements in target fragmentation treatments and computational efficiency are to be incorporated, even though computational execution times are already faster than

counterpart statistical (Monte Carlo) calculations. These improvements should not greatly alter the current results, and the present interim version of the GCR code should provide a reasonable estimate of cosmic ray particle fluxes and the corresponding dose predictions.

The absorbed dose  $D$  due to energy deposition at a given location  $x$  by all particles is calculated according to

$$D(x) = \sum_j \int_0^{\infty} S_j(E) \Phi_j(x, E) dE \quad \text{rad} \quad (2)$$

The degree to which biological systems undergo damage by ionizing radiation is not simply proportional to this absorbed dose for all particle types. For human exposure, the dose equivalent is defined by introducing the quality factor  $Q$  which relates the biological damage incurred due to any ionizing radiation to that produced by soft X rays. In general,  $Q$  is a function of linear energy transfer (LET), which in turn is a function of both particle type and energy. For the present calculations, the quality factors used are those specified by the International Commission on Radiological Protection (ref. 18). The dose equivalent,  $H$ , values are computed as

$$H(x) = \sum_j \int_0^{\infty} Q_j(E) S_j(E) \Phi_j(x, E) dE \quad \text{rem} \quad (3)$$

These are the values used to specify radiation exposure limits.

Maximum dose equivalent limits permissible for United States astronauts are recommended by the National Council on Radiation Protection and Measurement. These limits include dose values for the skin, ocular lens, and vital organs (ref. 19). For high-energy radiation from galactic cosmic rays and large solar flare ions, the dose delivered to the vital organs is the most important with regard to latent carcinogenic effects. This dose value is often referred to as the blood-forming organ (BFO) dose. When detailed body geometry is not considered, the BFO dose is usually computed as the dose incurred at a 5-cm depth in human tissue. For the BFO dose calculations in this analysis, the human tissue is simulated by 5 cm of water. Dose equivalent limits are established for short-term (30 day) exposures, annual exposures, and total career exposure. The 30-day BFO limit for United States astronauts is presently 25 rem (0.25 Sv), and the annual limit is set at 50 rem (0.5 Sv). Total career limits vary between 100 and 400 rem (1 and 4 Sv) depending upon age and gender.

## Transport Computational Results

The BRYNTRN code and the combined nucleon/heavy ion transport code are easily applied to the carbon dioxide medium. The code inputs of the initial particle fluxes through the medium are the GCR and solar flare flux-energy distributions as shown in figures 1 and 2. Results are presented in two forms. They include the slab calculations of the particle flux-energy distributions at various carbon dioxide absorber amounts and slab-dose estimates as a function of carbon dioxide absorber amount. The slab calculations correspond to a monodirectional beam of particles normally incident on a planar layer of shield material. The presentation of results in this form can be useful in estimating anticipated doses for various atmospheric models providing a different total shield protection (i.e., g/cm<sup>2</sup> of CO<sub>2</sub>) than those described in this analysis.

### Galactic Cosmic Ray Results

The GCR constituents in free space can have extremely high energies (>1 GeV) and, in addition to having high penetrating ability, they cause numerous nuclear reactions in absorbing media. Thus, the radiation field undergoes substantial changes in propagating through matter. The yearly differential flux as a function of energy for particles at 10, 50, and 100 g/cm<sup>2</sup> depth in carbon dioxide is shown in figures 6, 7, and 8, respectively. Although the code simulates the transport of particles of charge 0, 1, 2, . . . , 28 individually, the flux and dose contributions are presented as five entities for convenience of illustration: neutrons, protons, alpha particles, lighter nuclei ( $3 \leq Z \leq 9$ ), and heavier nuclei ( $10 \leq Z \leq 28$ ). By comparing the flux-energy distributions at 10, 50, and 100 g/cm<sup>2</sup>, the increase in flux of the lower energy neutrons and protons arises as a result of the fragmentation of the heavier ions. These basic flux-energy data are required to evaluate the corresponding dosimetric quantities as calculated in equations (2) and (3).

Dose values (rad) are determined from the particle differential fluxes at specific positions in the shield medium. The skin and BFO dose rates as a function of CO<sub>2</sub> absorber amount are shown in figures 9 and 10, respectively. The BFO results represent the dose evaluated after traverse of a given absorber amount of CO<sub>2</sub> with an additional 5-cm tissue layer (water) included. The difference between the corresponding skin doses and BFO doses is indicative of the self-shielding effect of the human body. From figures 9 and 10, the proton dose dominates through the first 100 g/cm<sup>2</sup> of material. The skin and the corresponding BFO dose equivalents (rem) are shown in fig-

ures 11 and 12, respectively. The dose equivalent values, being higher than the dose values of figures 9 and 10, illustrate the large impact of the quality factors on the actual damage incurred. As shown in figures 11 and 12, for approximately the first 10 g/cm<sup>2</sup> of CO<sub>2</sub>, the largest dose equivalent contributors are the heavier ions ( $10 \leq Z \leq 28$ ), with their relative importance rapidly decreasing thereafter. After approximately 40 g/cm<sup>2</sup>, nearly all the incurred dose equivalent is dominated by the protons and neutrons. The dose and dose equivalent values shown in figures 9 to 12 at 0 g/cm<sup>2</sup> of CO<sub>2</sub> correspond to the free-space dose and dose equivalent values. (In figs. 9 to 12, each curve represents the cumulative dose due to all contributors beneath, with the top curve representing the total dose.)

### Solar Flare Results

The manner in which solar flare particle energy is attenuated by matter is very sensitive to the energy spectrum of the particles incident on the atmosphere. For the three large proton flares analyzed, the quantity of high-energy particles (>100 MeV) varied inversely with the total proton flux; that is, the flares with initially more total protons had relatively fewer high-energy particles. (This was the case with the August 1972 event.) Since the higher energy particles are more proficient in generating secondary nucleons, those flares with lower total particles in free space may produce relatively high fluxes after interaction with the attenuating medium. The flux of nucleons as a function of carbon dioxide absorber amount is plotted for several particle energies for each of the three flares in figures 13, 14, and 15. The relatively rapid attenuation of the proton flux for the August 1972 spectrum (fig. 13) is indicative of its relative deficiency in high-energy particles. As a consequence, the neutrons produced (fig. 13(b)) are most abundant at low energies. However, once generated, these uncharged neutrons attenuate very slowly. The November 1960 flare results (fig. 14) show the influence of larger numbers of higher energy incident protons. For carbon dioxide absorber amounts greater than 20 g/cm<sup>2</sup>, protons with approximately 50 MeV energy predominate. In addition, the neutron spectrum at 80 to 100 g/cm<sup>2</sup> exhibits substantially more high-energy components than the corresponding August 1972 values. The highly penetrating spectrum of the February 1956 event serves to further accentuate the importance of the high-energy portion of the initial spectrum (fig. 15). For this event, proton fluxes are decreasing very gradually even at 100 g/cm<sup>2</sup>, while 100-MeV neutrons are still shown to be increasing.

The dosimetric quantities evaluated from the propagating flux distributions are given as a

function of carbon dioxide absorber amount in figures 16 to 19. The skin dose variation is shown in figure 16 for the three flares, and the corresponding skin dose equivalent variation is shown in figure 17. Note that for absorber amounts greater than about 30 g/cm<sup>2</sup>, dose values resulting from the February 1956 event are highest, whereas for 20 g/cm<sup>2</sup> and less, this flare results in the least incurred dose. The August 1972 flare produces extremely high doses at low absorber amounts. There is a smaller difference between the dose values (rad) and the corresponding dose equivalent values (rem) for the solar flare spectra as compared to the GCR spectra because of the higher quality factors of the heavy ion GCR constituents. For the solar flare events, the influence of the quality factor is more pronounced for solar events with higher energy spectra, since more neutrons are generated which have high quality factor values at medium and high energies (10 to 100 MeV). The BFO dose and dose equivalent variations are given in figures 18 and 19, respectively. The body's self-shielding influence becomes of less importance as the carbon dioxide absorber amount increases, since higher energy secondaries are responsible for most of the dose at larger thicknesses.

### Dose Predictions Near Mars Surface

When the computed propagation data for GCR and solar flare protons in carbon dioxide are applied to the Mars atmosphere models using the above approach, the doses incurred at various altitudes can be estimated. To evaluate the dose at a particular altitude or target point, the radiation from all directions must be determined. In these calculations, a spherically concentric atmosphere has been assumed. This geometry is illustrated in figure 20. The dosimetric values at a given target point are computed for carbon dioxide absorber amounts along slant paths through the atmosphere. For a target point at altitude  $h$  above the surface, the distance  $s$  along a slant path with zenith angle  $\theta$  is given by

$$s(z, \theta) = \sqrt{(R+h)^2 \cos^2 \theta + [2R(z-h) + z^2 - h^2]} - (R+h) \cos \theta \quad (4)$$

where  $z$  is the vertical altitude. The absorber amount along the slant path is then

$$\tau(h, \theta) = \frac{M_{\text{CO}_2}}{N_A} \int_0^\infty c(s) ds \quad \text{g/cm}^2 \quad (5)$$

For a given target point, the absorber amounts and the corresponding dosimetric quantities are evaluated for zenith angles between 0° and 90° in 5° increments.

The directional dose patterns produced are azimuthally symmetric. Sample directional patterns for the GCR and flare doses using the low-density atmosphere model for altitudes of 0 and 8 km above the surface are shown in figures 21 and 22, respectively. Each vector from the target point is proportional to the dose value per steradian incurred. The radiation with the higher energy spectra (GCR and the February 1956 flare) exhibits patterns more characteristic of a hemispherical distribution because of the greater penetration of the incident flux along all directions. The less penetrating August 1972 flare particles are substantially attenuated for large zenith angles, with most of the incurred dose coming from the overhead direction. The influence of altitude is readily seen by comparing the patterns of 0 km (fig. 21) with those of 8 km (fig. 22). (The dose patterns in figs. 21 and 22 have the same scale.) In particular, the August 1972 flare spectrum, which produced the lowest dose in figure 21, has become the largest of the sample doses at an 8-km altitude.

The total doses at a target point can now be found by the numerical integration of the dose values per steradian with respect to the solid angle over all directions. Integrated dose (rad) and dose equivalent (rem) calculations were made for both the high-density and the low-density atmosphere models at altitudes of 0, 4, 8, and 12 km. The decreasing protection provided by the atmosphere in the vertical direction at increasing altitudes is shown in table I.

Table I. Mars Atmospheric Protection in the Vertical Direction

Altitude, km	Protection, g/cm <sup>2</sup> CO <sub>2</sub>	
	Low-density model	High-density model
0	16	22
4	11	16
8	7	11
12	5	8

The corresponding dose values are shown in tables II, III, IV, and V. For GCR radiation, the BFO dose equivalent estimates at the surface range from approximately 10 to 12 rem/yr, with the total doses due to GCR changing very little at the higher altitudes investigated. For the August 1972 flare, the BFO dose equivalent estimates range from 2 to 5 rem/event at the surface with this value increasing significantly with altitude, up to 30 rem/event at 12 km. Thus, an unshielded dose of 30 rem is not unlikely during a large flare because of the large

Table II. Integrated Doses for the Mars Low-Density Atmosphere Model

		Integrated dose, rad, at altitude of—			
		0 km	4 km	8 km	12 km
Galactic cosmic ray	Skin	5.7	6.1	6.5	6.8
	BFO	5.5	5.9	6.2	6.5
Solar flare event 8/72	Skin	7.7	19.5	42.0	76.2
	BFO	3.7	8.5	16.4	27.3
Solar flare event 11/60	Skin	8.1	12.9	18.9	25.8
	BFO	6.0	9.1	12.6	16.4
Solar flare event 2/56	Skin	7.9	9.9	12.3	14.8
	BFO	7.1	8.5	10.0	11.4

Table III. Integrated Dose Equivalents for the Mars Low-Density Atmosphere Model

		Integrated dose equivalent, rem, at altitude of—			
		0 km	4 km	8 km	12 km
Galactic cosmic ray	Skin	13.2	15.9	18.9	22.4
	BFO	11.9	13.8	15.8	18.0
Solar flare event 8/72	Skin	9.0	21.9	46.2	82.6
	BFO	4.6	9.9	18.5	30.3
Solar flare event 11/60	Skin	9.7	15.1	21.9	29.6
	BFO	7.3	10.8	14.8	19.1
Solar flare event 2/56	Skin	11.0	13.4	16.2	19.1
	BFO	9.9	11.8	13.6	15.3

Table IV. Integrated Doses for the Mars High-Density Atmosphere Model

		Integrated dose, rad, at altitude of—			
		0 km	4 km	8 km	12 km
Galactic cosmic ray	Skin	5.3	5.7	6.1	6.4
	BFO	5.1	5.5	5.9	6.2
Solar flare event 8/72	Skin	3.1	8.1	18.7	38.9
	BFO	1.7	3.9	8.2	15.3
Solar flare event 11/60	Skin	5.2	8.3	12.6	18.2
	BFO	4.0	6.2	8.9	12.2
Solar flare event 2/56	Skin	6.5	8.0	9.8	12.0
	BFO	5.9	7.1	8.4	9.9

Table V. Integrated Dose Equivalents for the Mars High-Density Atmosphere Model

		Integrated dose equivalent, rem, at altitude of—			
		0 km	4 km	8 km	12 km
Galactic cosmic ray	Skin	11.3	13.4	15.8	18.6
	BFO	10.5	12.0	13.7	15.6
Solar flare event 8/72	Skin	3.9	9.5	21.1	42.8
	BFO	2.2	4.8	9.5	17.4
Solar flare event 11/60	Skin	6.4	10.0	14.8	21.1
	BFO	5.0	7.5	10.6	14.4
Solar flare event 2/56	Skin	9.2	11.1	13.3	15.9
	BFO	8.5	10.0	11.7	13.4

topographical relief present on the Martian surface. This BFO dose equivalent is above the permissible 30-day limit (25 rem). However, as shown in figure 19, the August 1972 flare is rapidly attenuated by matter and a few  $\text{g}/\text{cm}^2$  of additional shielding should reduce the anticipated dose below the 30-day limit. For the flare event of November 1960, the BFO dose equivalent estimates range from approximately 5 to 7 rem/event at the surface with values ranging up to 19 rem at a 12-km altitude. For the flare event of February 1956, BFO dose equivalent estimates range from approximately 8 to 10 rem/event, with the values ranging up to 15 rem at a 12-km altitude. From these results, a total yearly dose may be conservatively estimated as the sum of the annual GCR dose and the dose due to one large flare. At the surface, such an estimated dose equivalent is 19 to 22 rem/yr. At an altitude of 12 km, the estimated dose equivalent is 33 to 48 rem/yr. These values are below the 50 rem/yr BFO dose equivalent limit permissible for United States astronauts.

Some earlier and very preliminary dose estimates for manned Mars missions have been made for GCR and flare doses (refs. 20 and 21). A few general comparisons of their previous estimates may be made with the present results. The same GCR source spectrum is used in all analyses, and the August 1972 flare is included in the results of reference 20. However, both references 20 and 21 assumed a vertical carbon dioxide absorber amount of  $10 \text{ g}/\text{cm}^2$  in evaluating the Mars surface doses. Since the present calculations at a 4-km altitude for the low-density atmosphere model correspond to a vertical carbon dioxide absorber amount of  $10.9 \text{ g}/\text{cm}^2$ , these results should be comparable with those of references 20 and 21. From table III, the GCR skin and BFO dose equivalent values at 4 km are given as 15.9 and 13.8 rem/yr, respectively. The corresponding values in references 20 and 21 are comparable at 12 and 10 rem/yr, respectively. The somewhat higher values of the present calculations may be indicative of the very comprehensive nuclear interaction and fragmentation cross-section data base used.

In comparing the dose estimates of the August 1972 flare of reference 20 with the corresponding present calculations, larger differences are found. In particular, the skin dose equivalent value of 83 rem (ref. 20) is much higher than the 4-km value of table III (22 rem). This difference may be reconciled by consideration of the geometric influence. Since normal-incident radiation attenuation for slab shields may be equated to isotropic radiation at the center of a spherically shielded volume for  $4\pi$  steradian, a rough first estimate for the Martian atmosphere shielding can be made by reducing the slab dose

calculations by 50 percent. If this approximation is made, the present calculations indicate approximately 80 rem as half of a slab dose equivalent for  $10 \text{ g}/\text{cm}^2$  depth in carbon dioxide (fig. 17). However, if the incident spectrum is such that the radiation field is very sensitive to absorber amounts (as is the August 1972 flare), then detailed geometric effects must be included in the dose estimates. It is felt that the 22-rem skin dose equivalent value is a more reasonable dose estimate for this flare at the 4-km level in the Martian atmosphere. For the same reasons, but to a lesser degree, it is believed that the BFO dose equivalent value for this flare is also overpredicted in reference 20 (17 rem versus 10 rem).

## Conclusions

Ionizing radiation exposure levels and corresponding dosimetric quantities have been estimated for conditions in the Martian atmosphere. The propagation of galactic cosmic and solar flare radiation in representative model Martian atmospheres has been predicted from calculations made with the Langley Research Center nucleon and heavy ion transport codes. It has been found that substantial shielding is provided by the tenuous Martian atmosphere and that variations with altitude are significant.

In the results given previously, one may construe a conservative yearly dose prediction as the sum of the annual galactic cosmic ray dose and the dose due to one large flare. For the most favorable shielding case (the high-density model at the surface), the total blood-forming organ (BFO) dose equivalent may approach 19 rem/yr. For the low-density, high-altitude (12 km) case, the annual BFO dose equivalent may be as high as 48 rem/yr. These dose predictions imply that the atmosphere of Mars may provide shielding sufficient to maintain the annual BFO dose levels below the current 50 rem/yr United States astronaut limit. However, it must be emphasized that the foregoing results are preliminary and should be considered as current state-of-the-art "best estimates." Furthermore, it must be realized that Mars exploration crews are likely to incur a substantial dose while in transit to Mars. Therefore, additional crew radiation protection on the Mars surface may be required. Thus, one may conclude that even though the Martian atmosphere does provide a significant amount of radiation protection, some additional shielding may be desirable for extended manned presence on Mars.

NASA Langley Research Center  
Hampton, VA 23665-5225  
February 6, 1990

## References

1. Office of Exploration Study Requirements Document—FY 1989 Studies. Doc. No. Z-2.1-002, NASA, Mar. 3, 1989.
2. Adams, J. H., Jr.; Silberberg, R.; and Tsao, C. H.: *Cosmic Ray Effects on Microelectronics. Part 1: The Near-Earth Particle Environment*. NRL-MR-4506-PT-1, Naval Research Lab., Aug. 1981. (Available from DTIC as AD A103 897.)
3. Webber, W. R.: The Interstellar Cosmic Ray Spectrum and Energy Density—Interplanetary Cosmic Ray Gradients and a New Estimate of the Boundary of the Heliosphere. *Astron. & Astrophys.*, vol. 179, no. 1-2, June 1987, pp. 277-284.
4. *Interplanetary Charged Particle Models (1974)*. NASA SP-8118, 1975.
5. Švestka, Zdeněk: *Solar Flares*. D. Reidel Publ. Co., Inc., c.1976.
6. Wilson, John W.: Environmental Geophysics and SPS Shielding. *Workshop on the Radiation Environment of the Satellite Power System*, Walter Schimmerling and Stanley B. Curtis, eds., LBL-8581 (Contract W-7405-ENG-48), Univ. of California, Sept. 15, 1978, pp. 33-116.
7. Smith, Robert E.; and West, George S., compilers: *Space and Planetary Environment Criteria Guidelines for Use in Space Vehicle Development, 1982 Revision (Volume 1)*. NASA TM-82478, 1983.
8. Kaplan, David I., compiler: *Environment of Mars, 1988*. NASA TM-100470, 1988.
9. Hess, S. L.; Ryan, J. A.; Tillman, J. E.; Henry, R. M.; and Leovy, C. B.: The Annual Cycle of Pressure on Mars Measured by Viking Landers 1 and 2. *Geophys. Res. Lett.*, vol. 7, no. 3, Mar. 1980, pp. 197-200.
10. Mutch, Thomas A.; Arvidson, Raymond E.; Head, James W., III; Jones, Kenneth L.; and Saunders, R. Stephen: *The Geology of Mars*. Princeton Univ. Press, c.1976.
11. Wilson, John W.; Townsend, Lawrence W.; Nealy, John E.; Chun, Sang Y.; Hong, B. S.; Buck, Warren W.; Lamkin, S. L.; Ganapol, Barry D.; Khan, Ferdous; and Cucinotta, Francis A.: *BRYNTRN: A Baryon Transport Model*. NASA TP-2887, 1989.
12. Wilson, John W.; and Badavi, F. F.: Methods of Galactic Heavy Ion Transport. *Radiat. Res.*, vol. 108, 1986, pp. 231-237.
13. Wilson, J. W.; Townsend, L. W.; and Badavi, F. F.: Galactic HZE Propagation Through the Earth's Atmosphere. *Radiat. Res.*, vol. 109, no. 2, Feb. 1987, pp. 173-183.
14. Wilson, John W.: *Analysis of the Theory of High-Energy Ion Transport*. NASA TN D-8381, 1977.
15. Wilson, John W.; and Townsend, Lawrence W.: A Benchmark for Galactic Cosmic-Ray Transport Codes. *Radiat. Res.*, vol. 114, no. 2, May 1988, pp. 201-206.
16. Townsend, Lawrence W.; and Wilson, John W.: *Tables of Nuclear Cross Sections for Galactic Cosmic Rays—Absorption Cross Sections*. NASA RP-1134, 1985.
17. Wilson, J. W.; Townsend, L. W.; Buck, W. W.; Chun, S. Y.; Hong, B. S.; and Lamkin, S. L.: *Nucleon-Nucleus Interaction Data Base: Total Nuclear and Absorption Cross Sections*. NASA TM-4053, 1988.
18. *Recommendations of the International Commission on Radiological Protection*. ICRP Publ. 26, Pergamon Press, Jan. 17, 1977.
19. Fry, R. J. M.; and Nachtwey, D. S.: Radiation Protection Guidelines for Space Missions. *Health Phys.*, vol. 55, no. 2, Aug. 1988, pp. 159-164.
20. Nachtwey, D. S.: Manned Mars Mission Radiation Environment and Radiobiology. *Manned Mars Missions Working Group Papers, Volume II*, NASA TM-89321, 1986, pp. 634-641.
21. Letaw, John R.; Silberberg, Rein; and Tsao, C. H.: Natural Radiation Hazards on the Manned Mars Mission. *Manned Mars Missions Working Group Papers, Volume II*, NASA TM-89321, 1986, pp. 642-655.

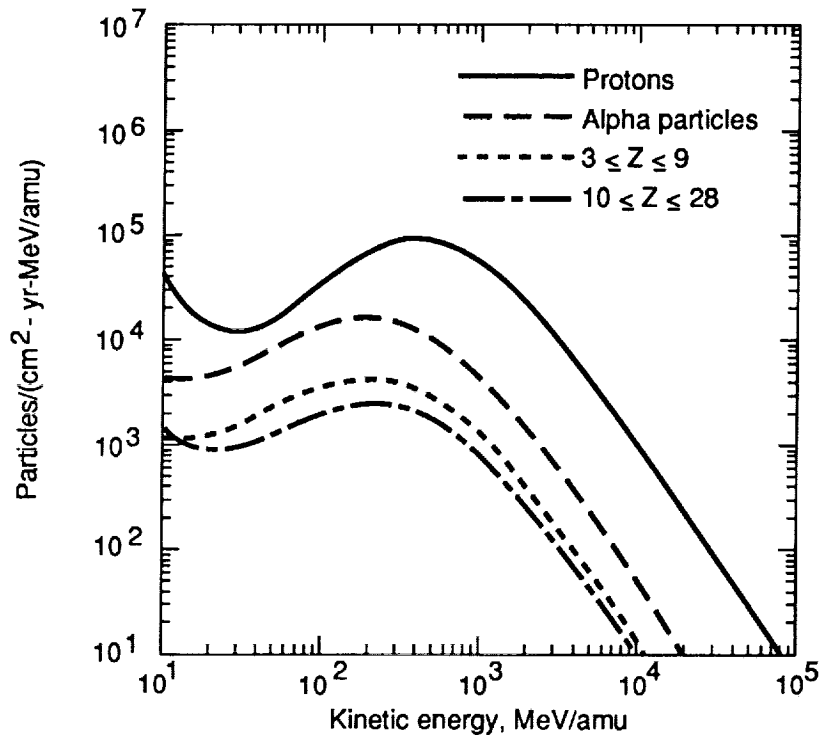


Figure 1. Flux versus energy distribution for galactic cosmic ray ions during solar minimum (data from ref. 2).

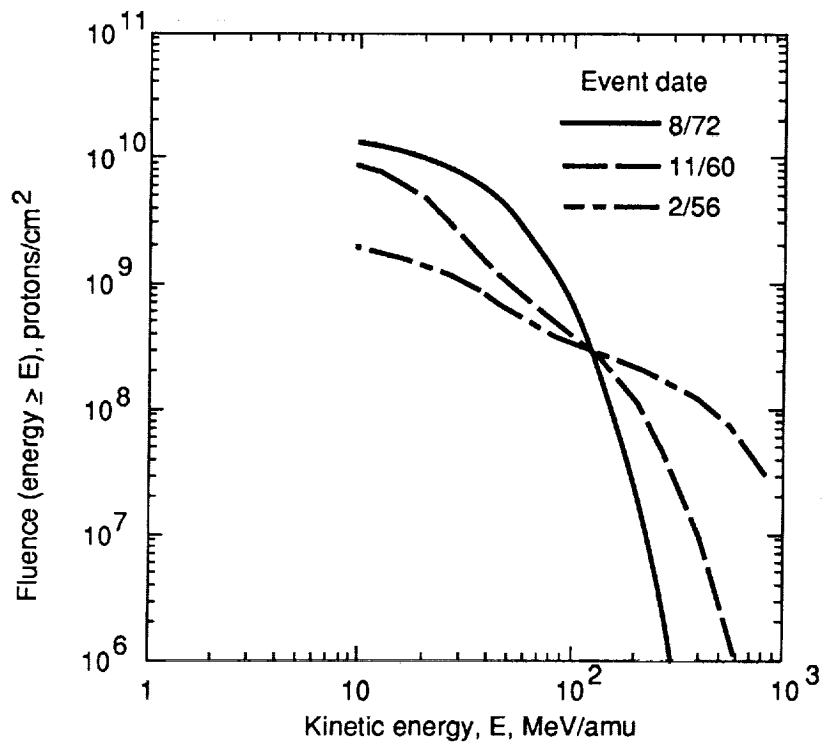
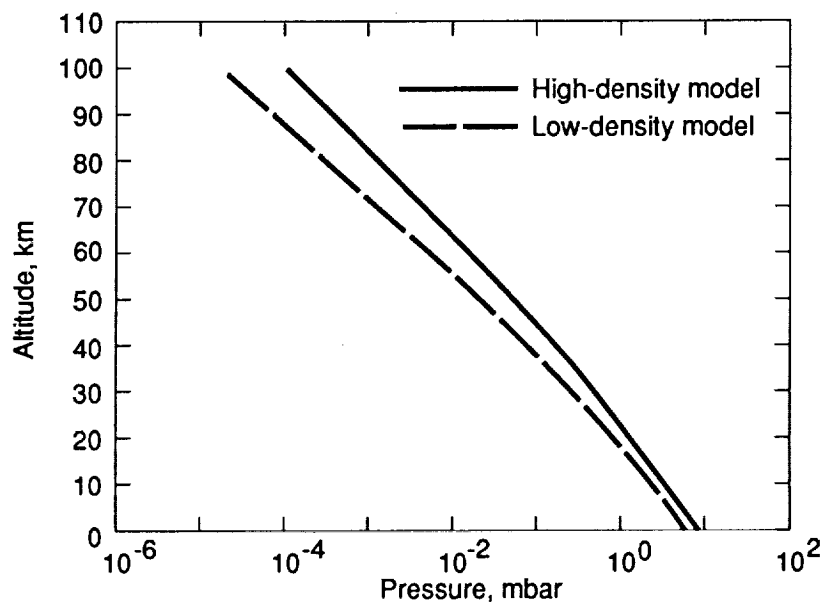
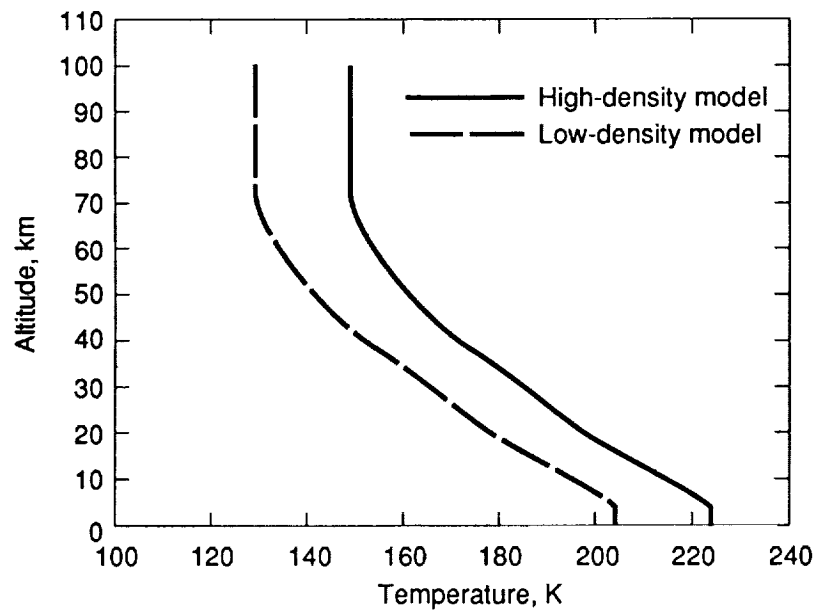


Figure 2. Integrated fluence spectra for three large solar proton flares (redrawn from ref. 6).



(a) Pressure profiles.



(b) Temperature profiles.

Figure 3. Vertical structure of Martian atmosphere models (data from ref. 7).

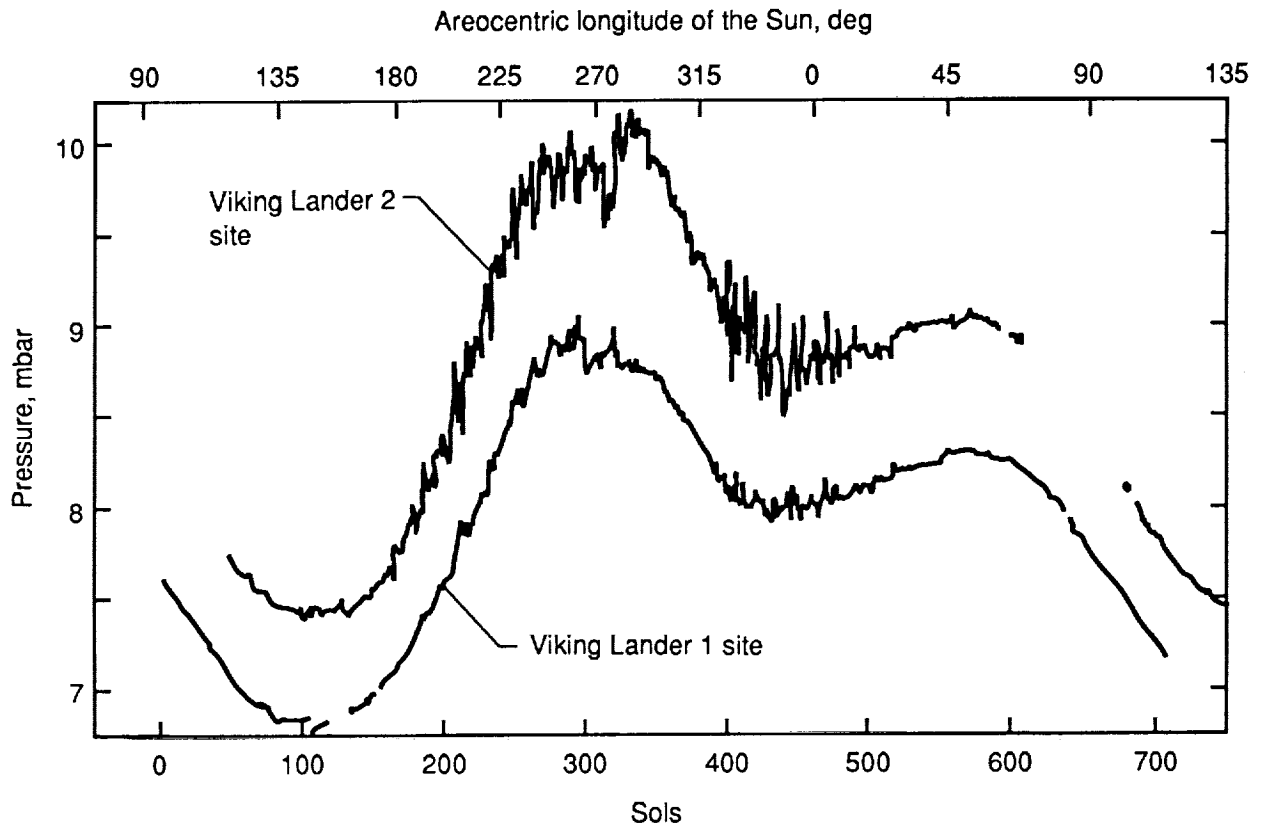


Figure 4. Daily mean pressure at the two Viking landing sites over 700 sols (redrawn from ref. 9).

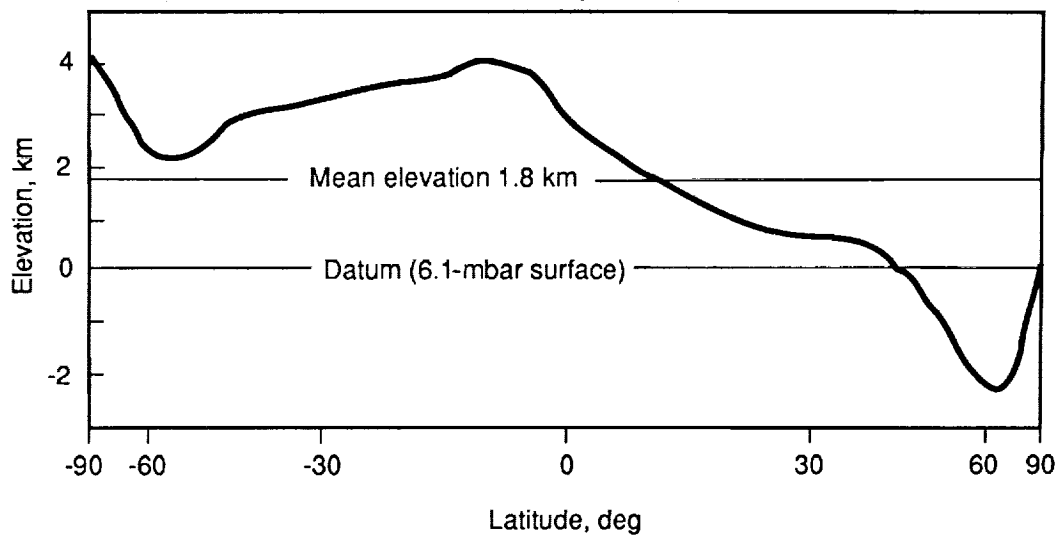


Figure 5. Average elevation of Mars latitude belts (redrawn from ref. 10).

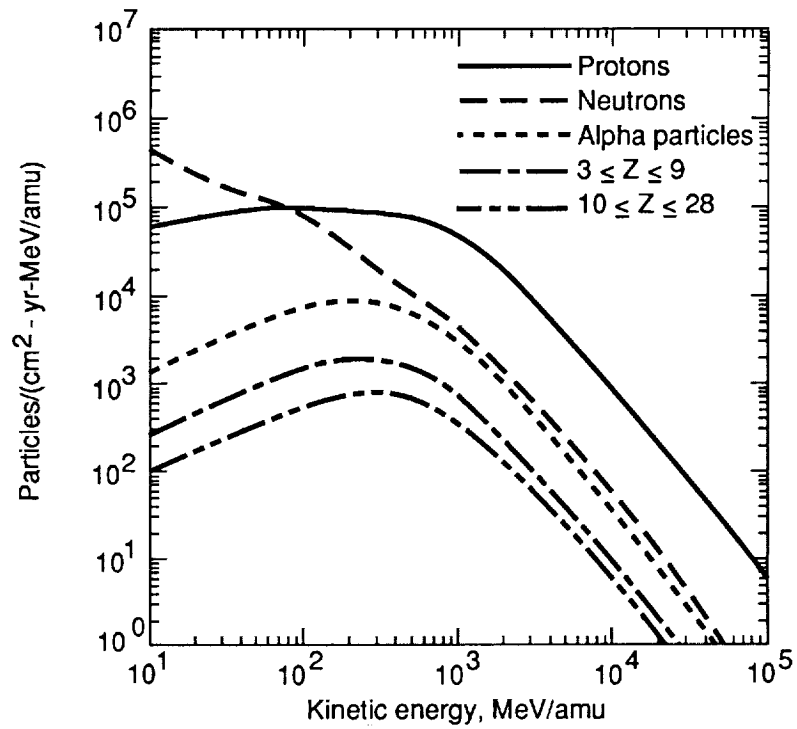


Figure 6. Yearly differential flux versus energy for particles at 10 g/cm<sup>2</sup> depth in carbon dioxide resulting from incident GCR at solar minimum.

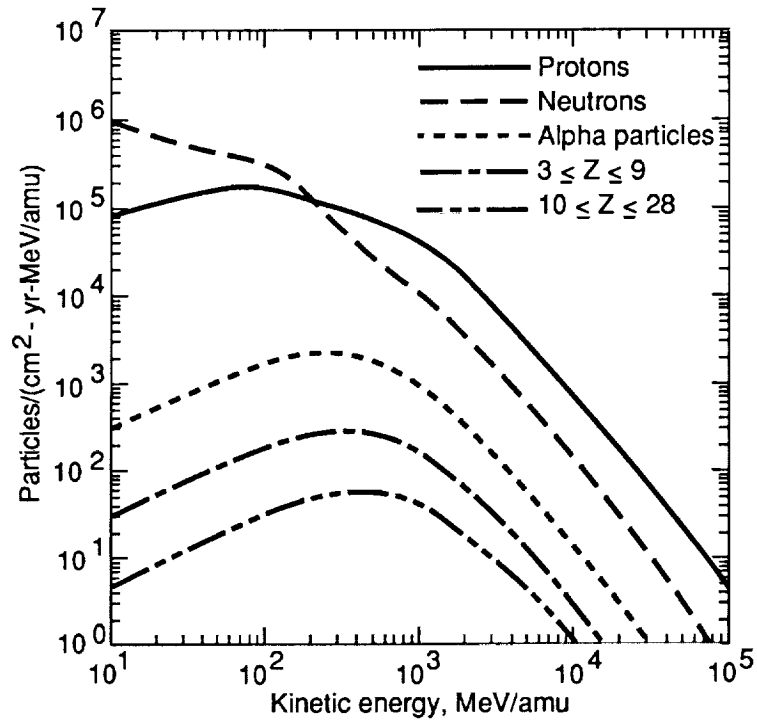


Figure 7. Yearly differential flux versus energy for particles at 50 g/cm<sup>2</sup> depth in carbon dioxide resulting from incident GCR at solar minimum.

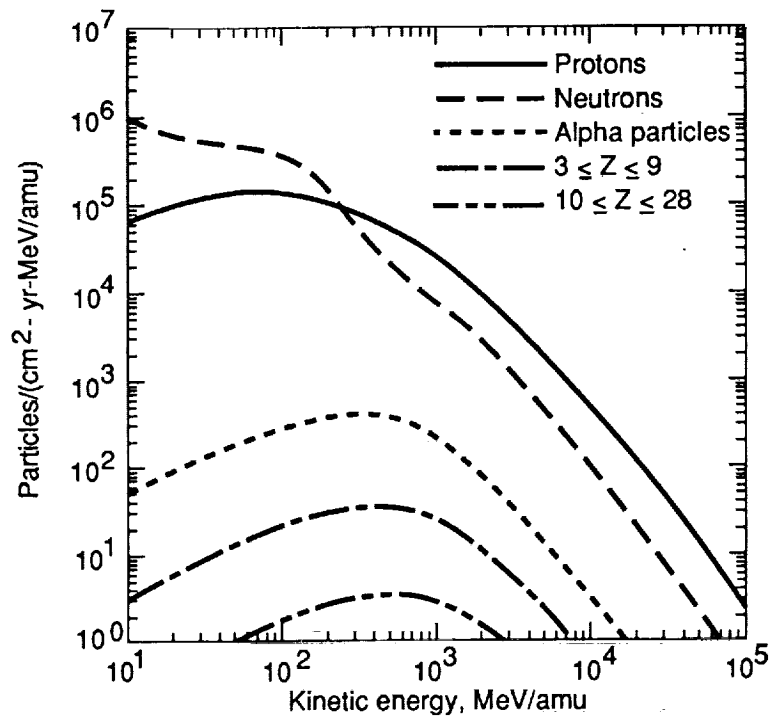


Figure 8. Yearly differential flux versus energy for particles at 100 g/cm<sup>2</sup> depth in carbon dioxide resulting from incident GCR at solar minimum.

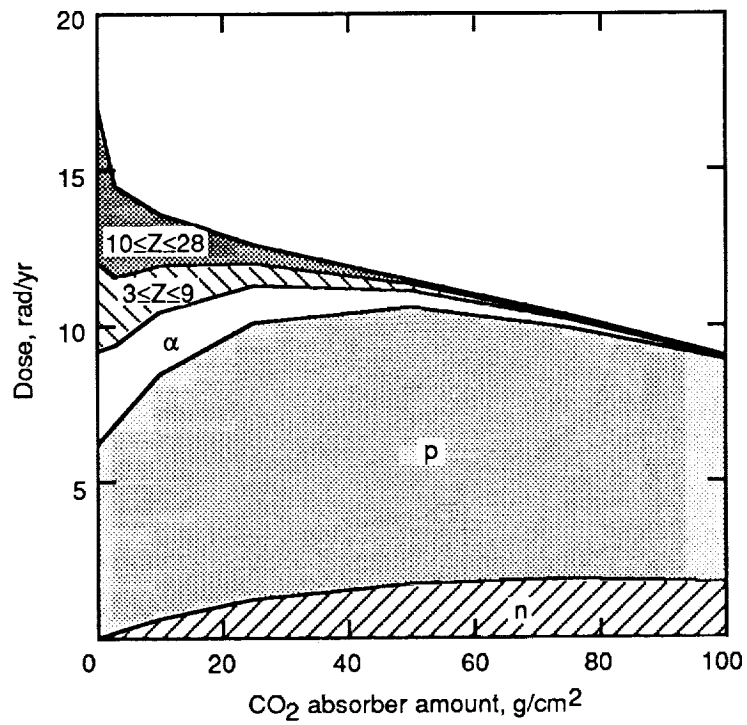


Figure 9. Annual skin dose contributions from specified particle constituents as a function of carbon dioxide absorber amount for GCR.

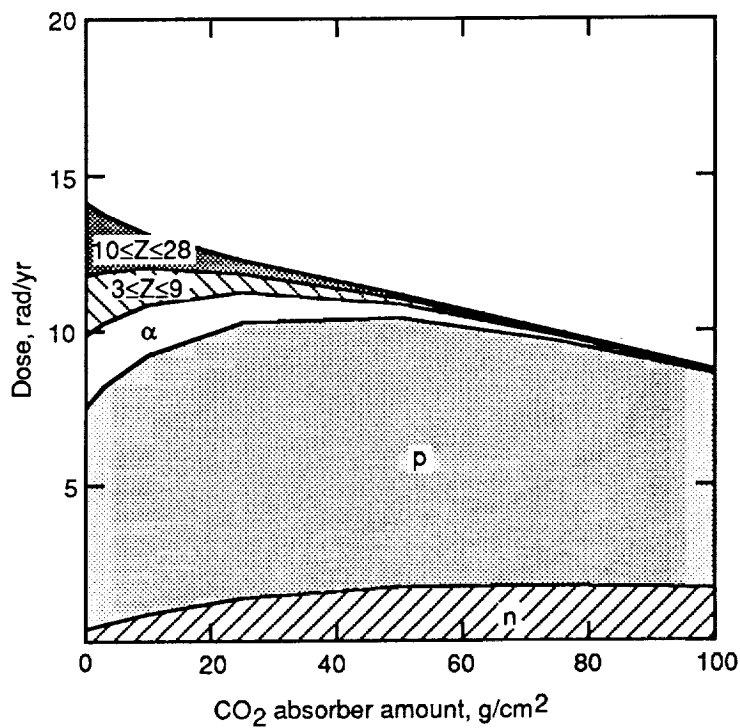


Figure 10. Annual BFO dose contributions from specified particle constituents as a function of carbon dioxide absorber amount for GCR.

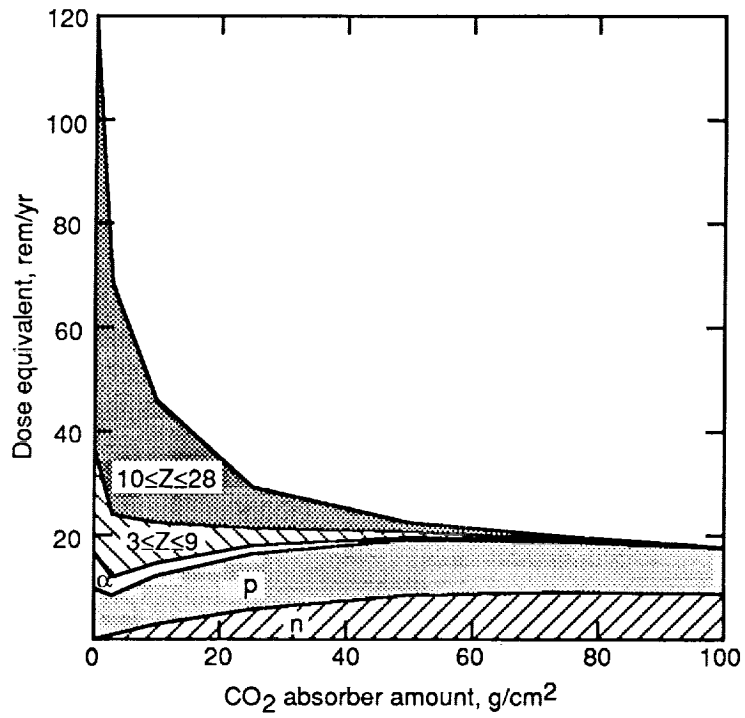


Figure 11. Annual skin dose equivalent contributions from specified particle constituents as a function of carbon dioxide absorber amount for GCR.

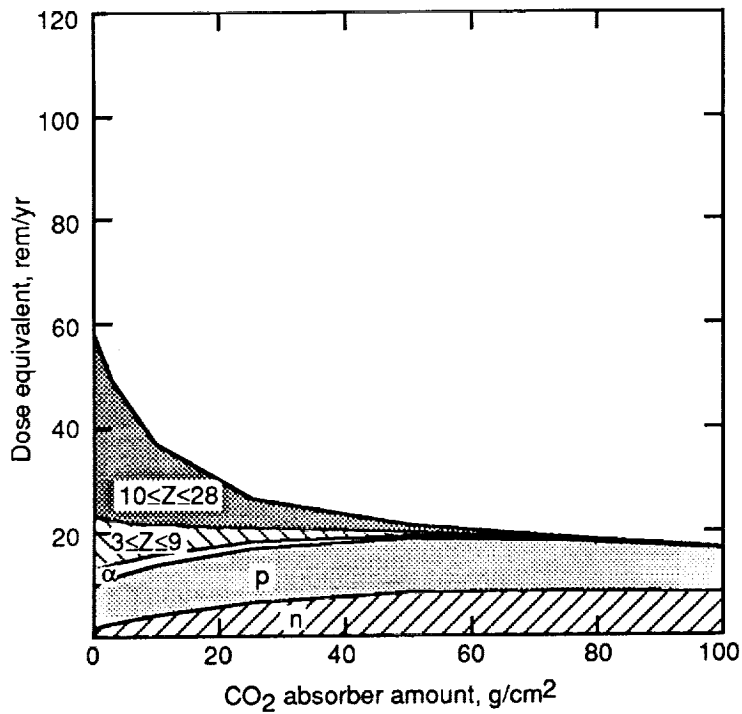
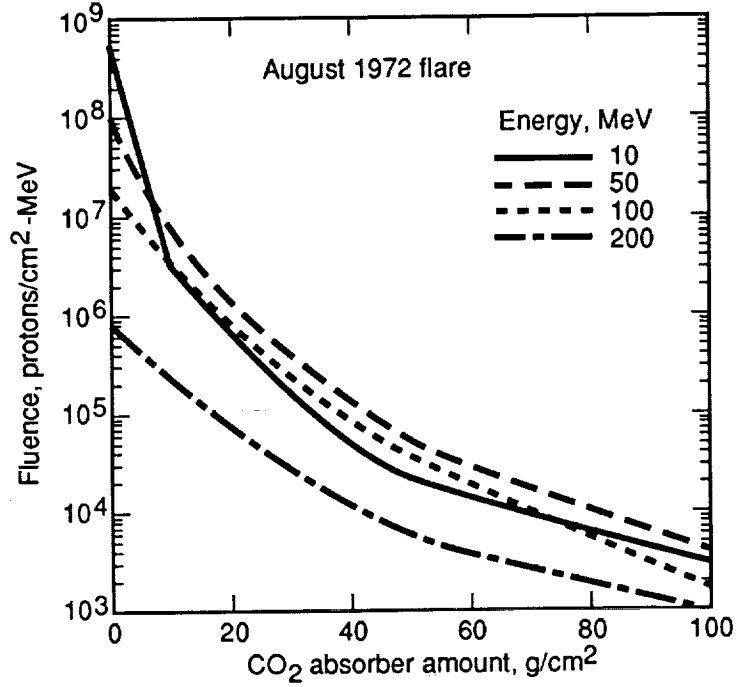
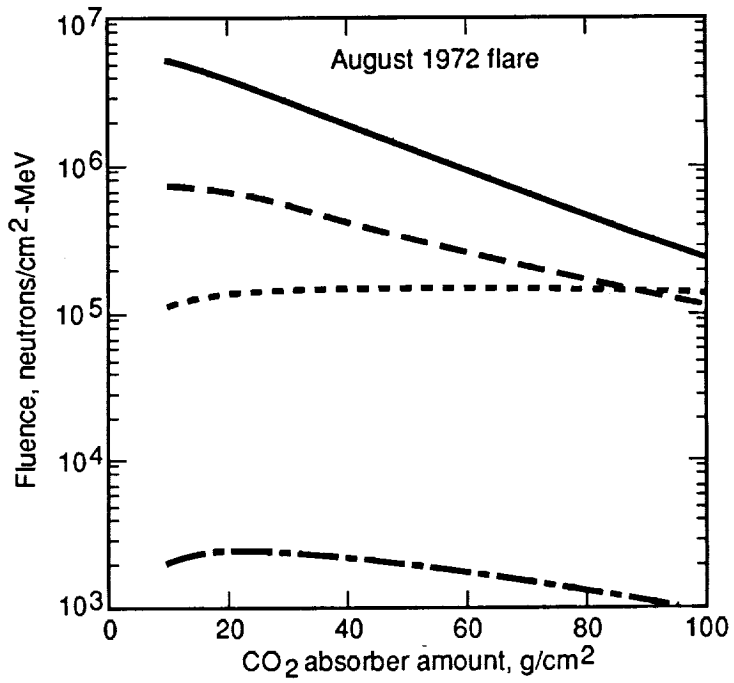


Figure 12. Annual BFO dose equivalent contributions from specified particle constituents as a function of carbon dioxide absorber amount for GCR.

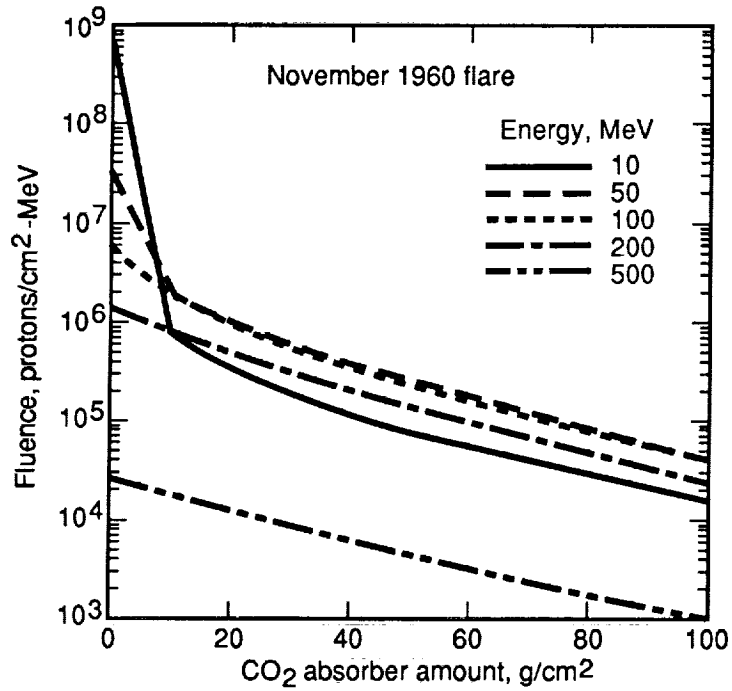


(a) Protons.

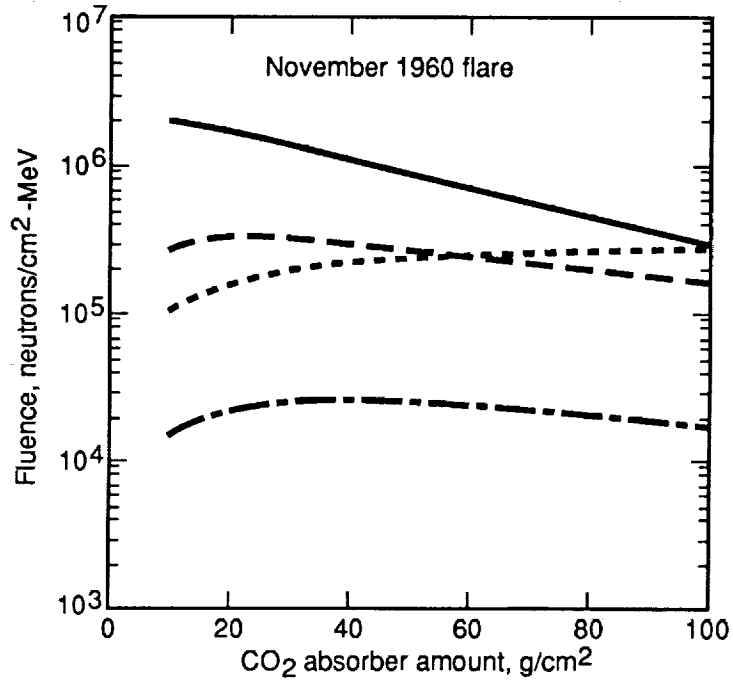


(b) Neutrons.

Figure 13. Fluence of protons and neutrons in CO<sub>2</sub> for the August 1972 flare spectrum.

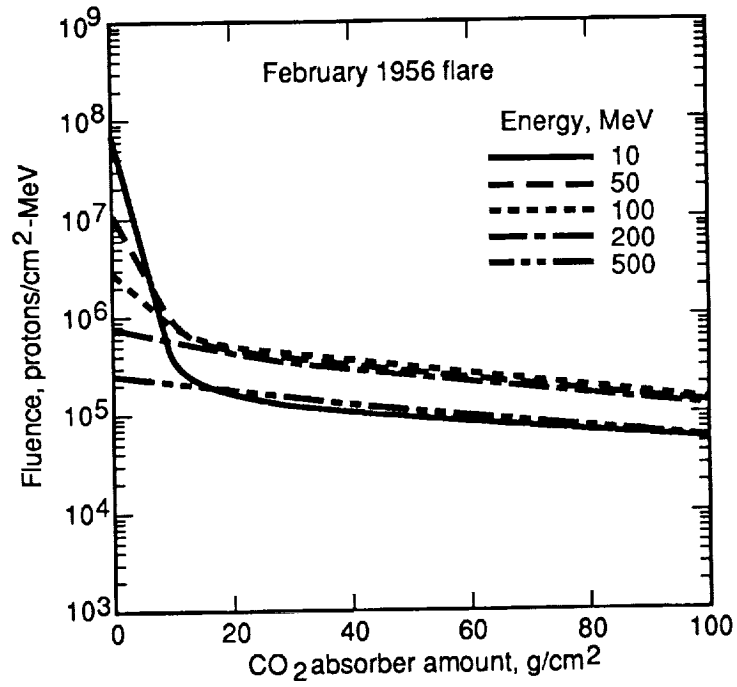


(a) Protons.

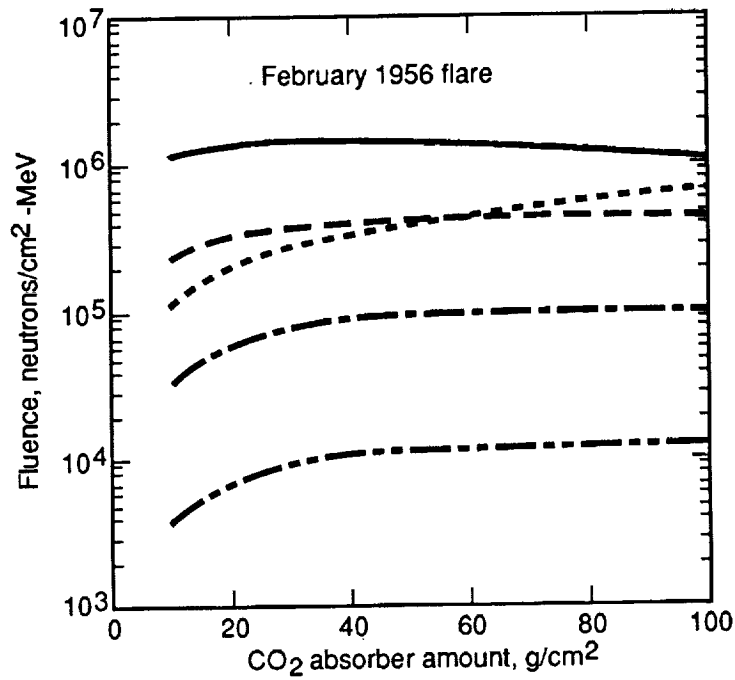


(b) Neutrons.

Figure 14. Fluence of protons and neutrons in CO<sub>2</sub> for the November 1960 flare spectrum.



(a) Protons.



(b) Neutrons.

Figure 15. Fluence of protons and neutrons in CO<sub>2</sub> for the February 1956 flare spectrum.

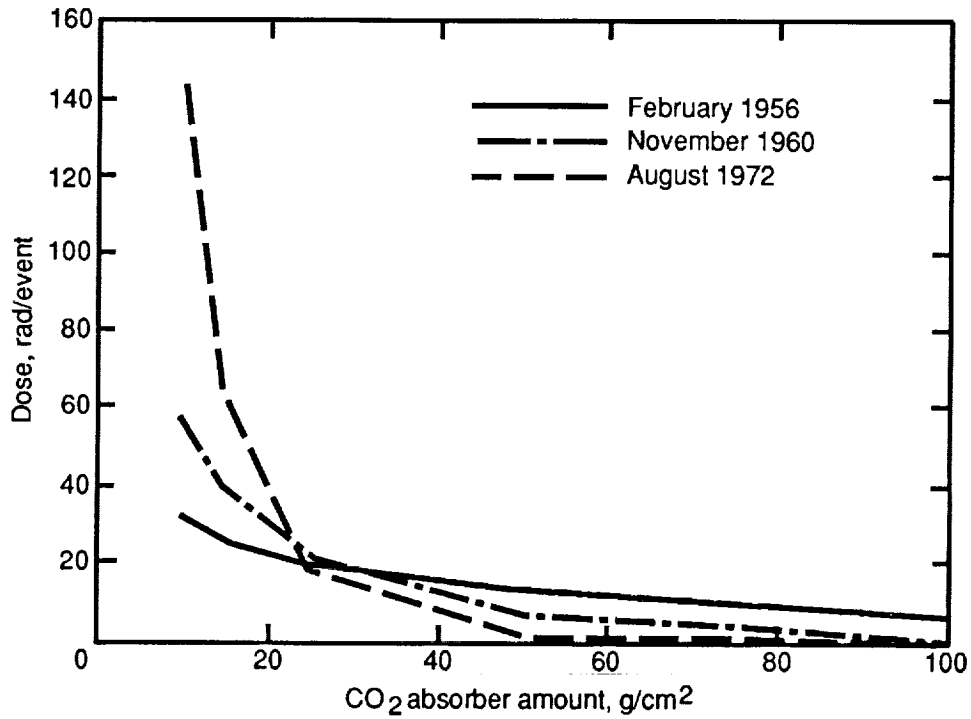


Figure 16. Skin dose as a function of carbon dioxide absorber amounts for three solar flare events.

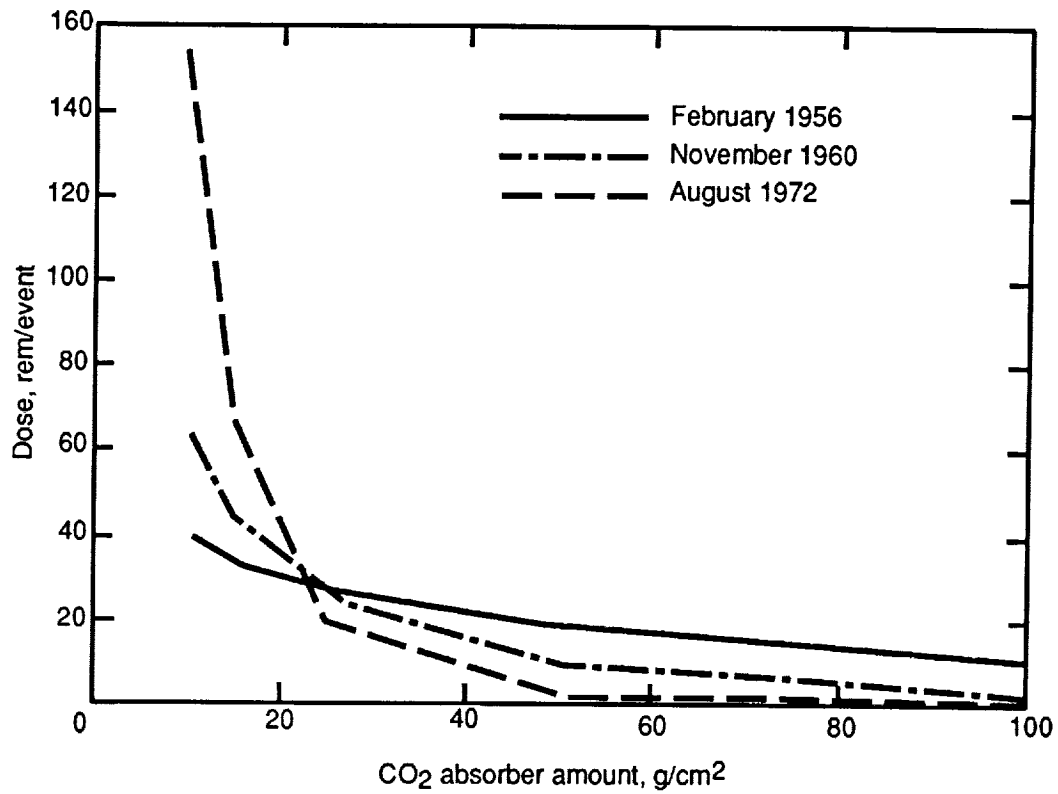


Figure 17. Skin dose equivalents as a function of carbon dioxide absorber amounts for three solar flare events.

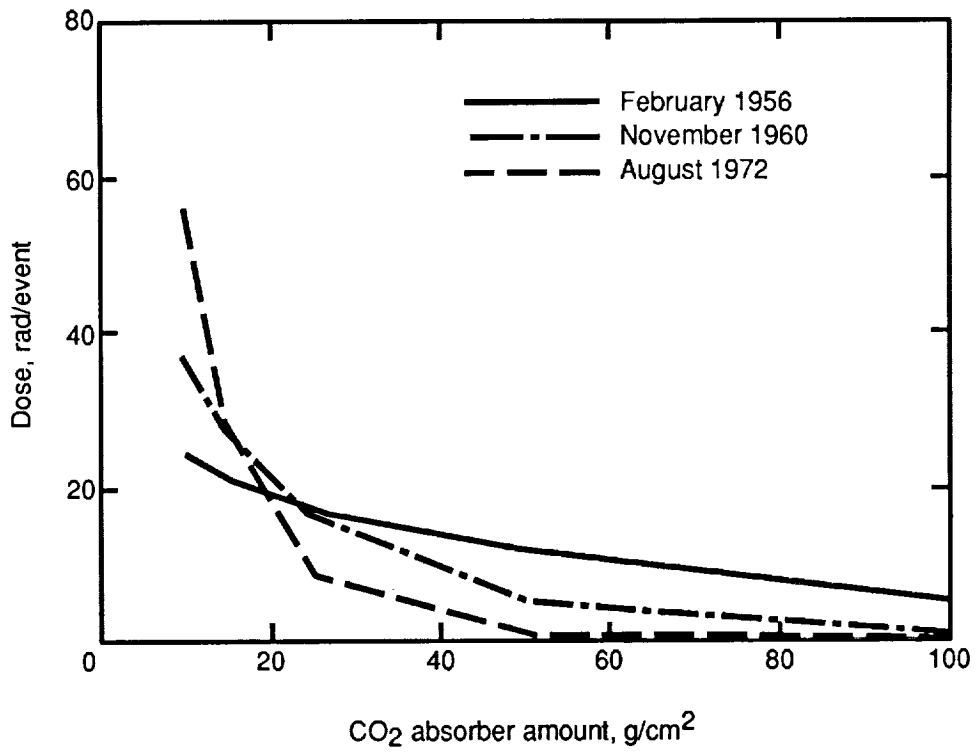


Figure 18. BFO dose as a function of carbon dioxide absorber amounts for three solar flare events.

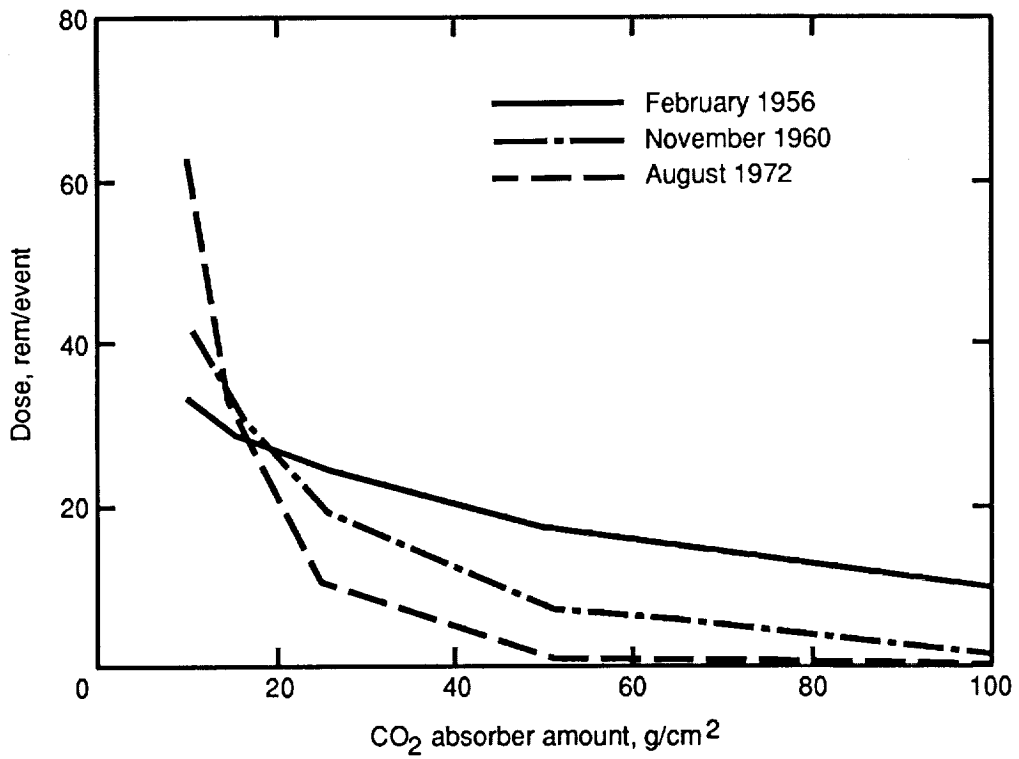


Figure 19. BFO dose equivalents as a function of carbon dioxide absorber amounts for three solar flare events.

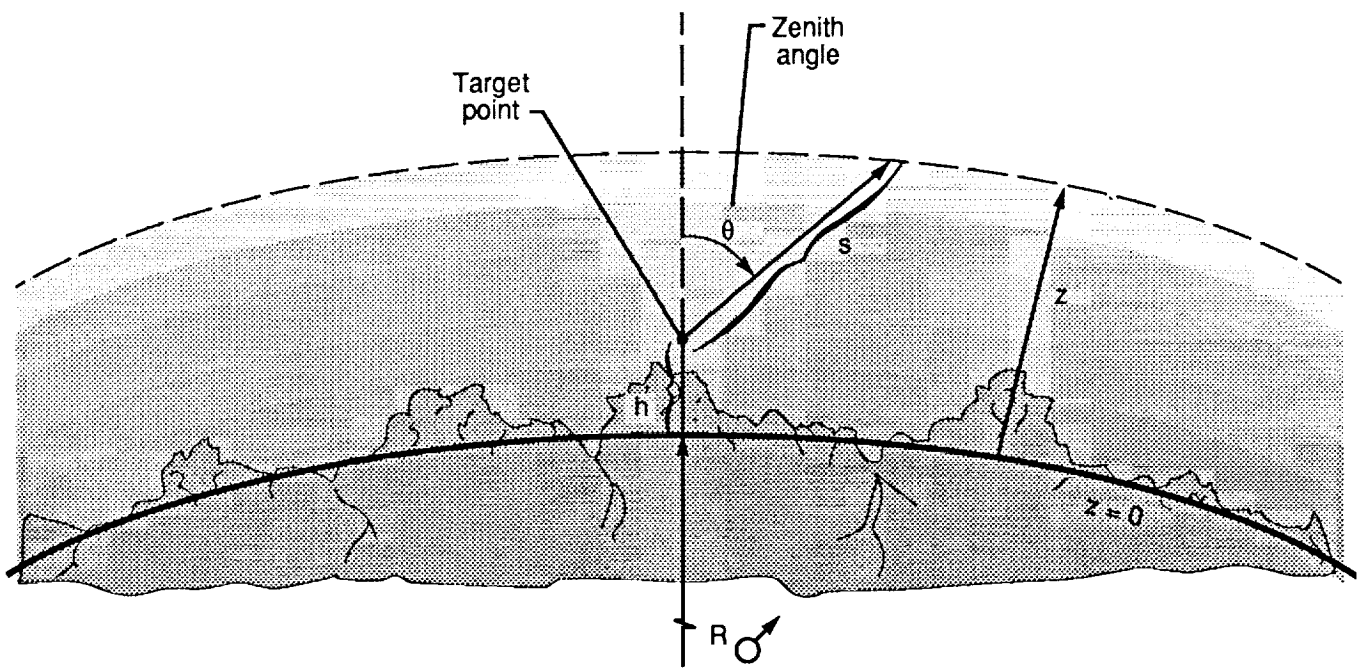


Figure 20. Depiction of Martian atmosphere geometry and parameters associated with dose calculations at a target point.

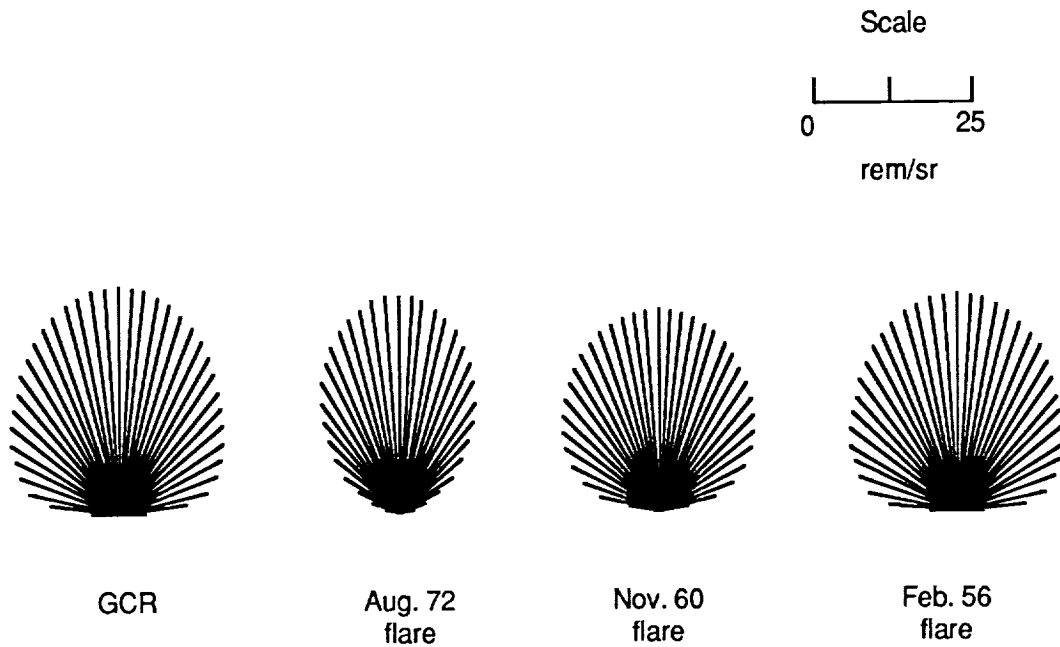


Figure 21. Directional BFO dose equivalent variation at the Martian surface for galactic cosmic rays and three solar flares. (Low-density atmospheric model results.)

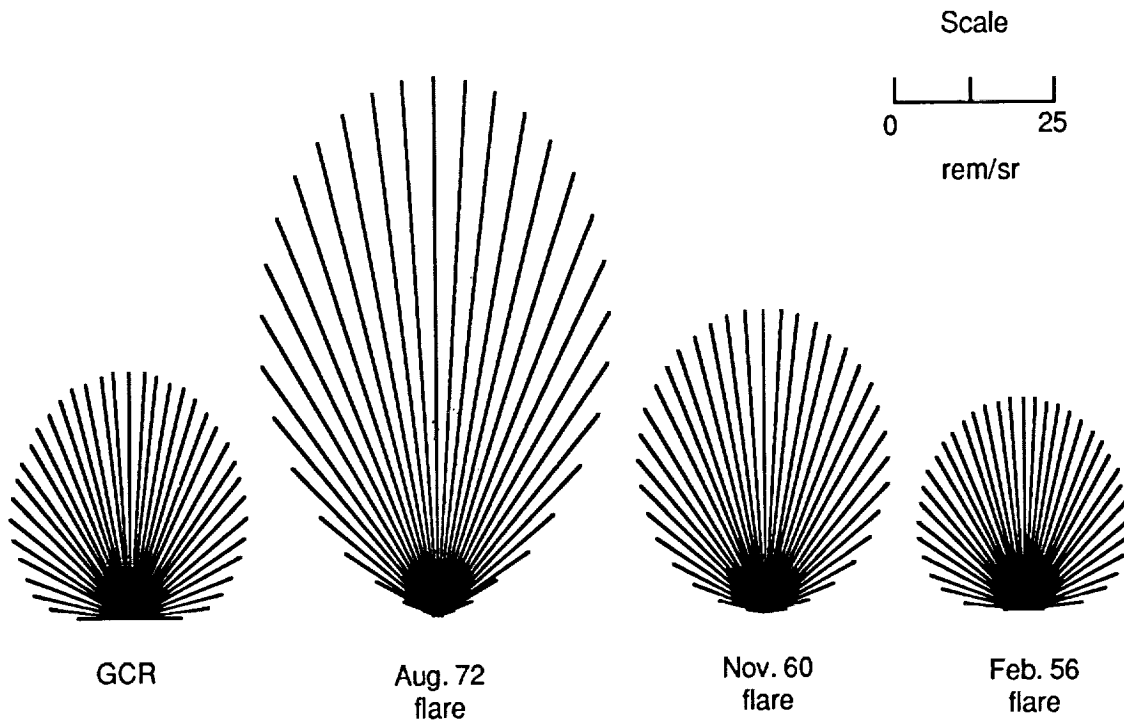
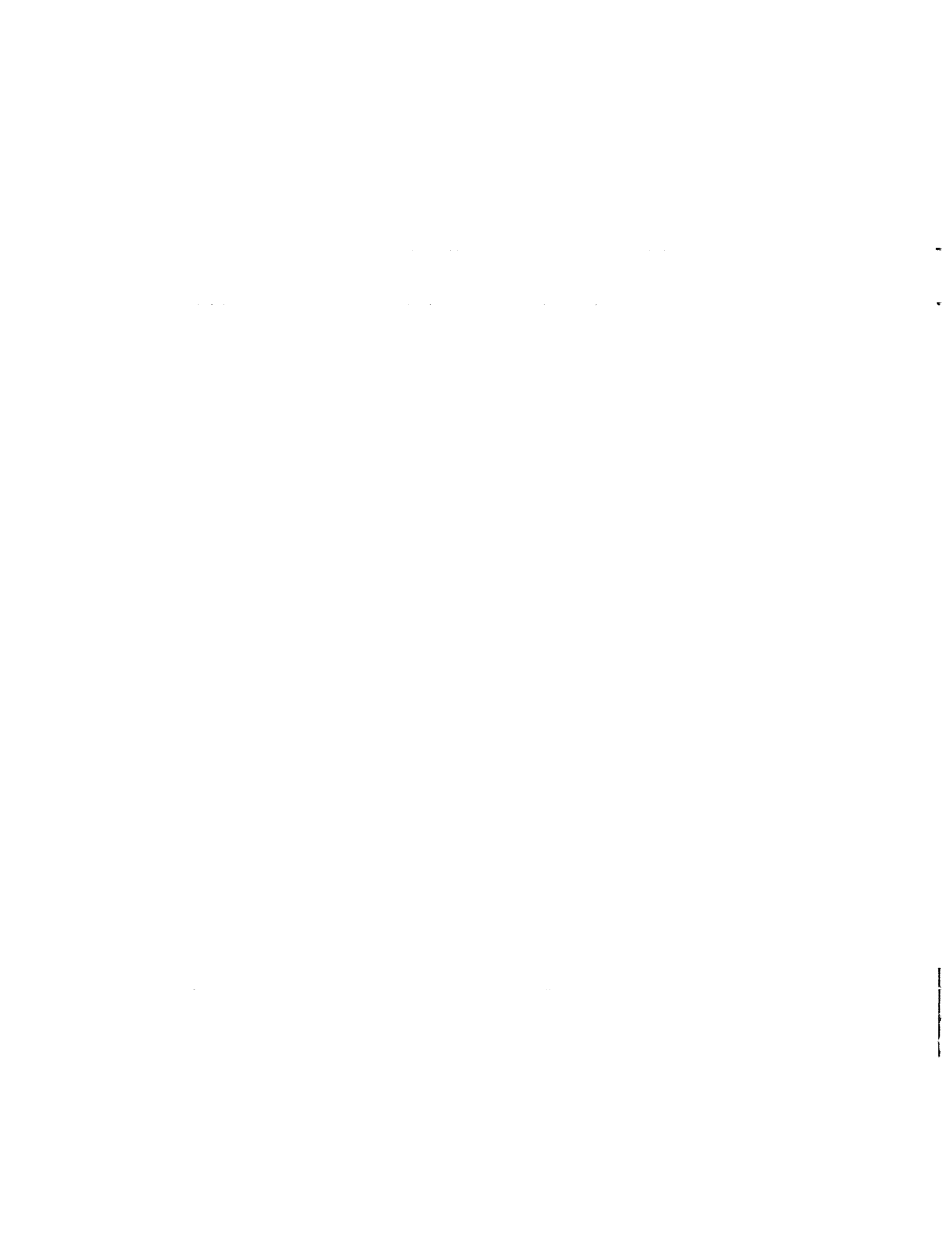


Figure 22. Directional BFO dose equivalent variation at an altitude of 8 km for galactic cosmic rays and three solar flares. (Low-density atmospheric model results.)





## Report Documentation Page

1. Report No. NASA TP-2979	2. Government Accession No.	3. Recipient's Catalog No.	
4. Title and Subtitle Radiation Exposure for Manned Mars Surface Missions		5. Report Date March 1990	6. Performing Organization Code
		8. Performing Organization Report No. L-16708	
7. Author(s) Lisa C. Simonsen, John E. Nealy, Lawrence W. Townsend, and John W. Wilson		10. Work Unit No. 326-22-20-50	11. Contract or Grant No.
9. Performing Organization Name and Address NASA Langley Research Center Hampton, VA 23665-5225		13. Type of Report and Period Covered Technical Paper	
		14. Sponsoring Agency Code	
12. Sponsoring Agency Name and Address National Aeronautics and Space Administration Washington, DC 20546-0001			
15. Supplementary Notes			
16. Abstract The Langley cosmic ray transport code and the Langley nucleon transport code (BRYNTRN) are used to quantify the transport and attenuation of galactic cosmic rays (GCR) and solar proton flares through the Martian atmosphere. Surface doses are estimated using both a low-density and a high-density carbon dioxide model of the atmosphere which, in the vertical direction, provide a total of 16 g/cm <sup>2</sup> and 22 g/cm <sup>2</sup> of protection, respectively. At the Martian surface during the solar minimum cycle, a blood-forming organ (BFO) dose equivalent of 10.5 to 12 rem/yr due to galactic cosmic ray transport and attenuation is calculated. Estimates of the BFO dose equivalents that would have been incurred from the three large solar flare events of August 1972, November 1960, and February 1956 are also calculated at the surface. Results indicate surface BFO dose equivalents of approximately 2-5, 5-7, and 8-10 rem per event, respectively. Doses are also estimated at altitudes up to 12 km above the surface where the atmosphere will provide less total protection.			
17. Key Words (Suggested by Authors(s)) Mars habitation Radiation exposure Solar flares Galactic cosmic rays		18. Distribution Statement Unclassified—Unlimited  Subject Category 93	
19. Security Classif. (of this report) Unclassified	20. Security Classif. (of this page) Unclassified	21. No. of Pages 24	22. Price A03

